Biopolymer Stabilization/Solidification of Soils: A Rapid, Micro-Macro, Cross-disciplinary approach.

Samuel J. Armistead,[1,2] Andrea Rawlings,[1] Colin C. Smith,[2*] Sarah S. Staniland[1*]

[1]Department of Chemistry, The University of Sheffield, Dainton Building, Brook Hill, Sheffield S3 7HF, UK

[2]Department of Civil and Structural Engineering, The University of Sheffield, Sir Frederick Mappin Building, Sheffield, S1 3JD, UK

*To whom correspondence should be addressed
E-mail: c.c.smith@sheffield.ac.uk, s.s.staniland@sheffield.ac.uk

ABSTRACT

In this study we describe a novel high throughput, micro-macro approach for the identification and efficient design of biopolymer stabilised soil systems. At the 'microscopic' scale we propose a rapid Membrane Enabled Bio-Mineral Affinity Screening (MEBAS) approach supported by Mineral Binding Characterization (MBC) (TGA, ATR-FTIR and Zeta Potential), while at the 'macroscopic' scale, micro scale results are confirmed by Geotechnical Verification (GV) through unconfined compression testing. We illustrate the methodology using an exemplar mine tailings Fe_2O_3 – SiO_2 system. Five different biopolymers were tested against Fe_2O_3: Locust Bean Gum, Guar Gum, Gellan Gum, Xanthan Gum and Sodium Carboxymethyl Cellulose. The screening revealed that Locust Bean Gum and Guar Gum have the highest affinity for Fe_2O_3, which was confirmed by MBC and GV. This affinity is attributed to the biopolymer's ability to form covalent C-O-Fe bonds through β-(1-4)-D-Mannan groups. Upon their 1% addition to a 'macroscopic' Fe_2O_3 based exemplar MT system, unconfined compressive strengths of 5171 kPa and 3848 kPa were obtained, significantly higher than for the other biopolymers and non-Fe systems. In the current study MEBAS gave an approximately 50-fold increase in rate of assessment compared to GV alone. Application of the proposed MEBAS – MBC - GV approach to a broad range of soil/earthwork components and additives is discussed.

Keywords. stabilization, solidification, biopolymer, bio-mineral, micro-macro.

TOC GRAPHIC
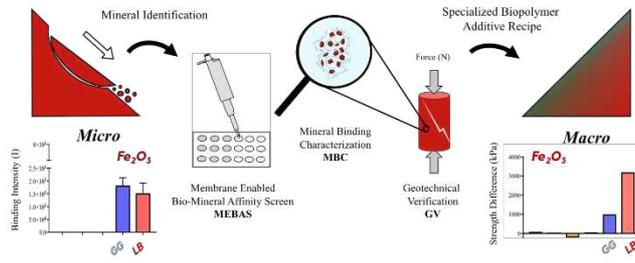
1. INTRODUCTION

Soil stabilization/solidification is a long-established methodology for improving weak soils during the construction of geotechnical structures such as foundations, roadbases, flood defences and larger structures such as slope embankments and tailings dams. Typically, engineers resort to the use of 7.5-10% Ordinary Portland Cement (OPC) to achieve adequate stabilization.[1] However cement accounts for 5% of global production of CO_2 with one ton of cement producing approximately one ton of CO_2.[2] As the climate crisis necessitates a move towards sustainable solutions, there will be increasing pressure to stabilise soils in many forms, whilst curtailing the use of cement.

The search for alternative stabilization/solidification mechanisms has attracted a variety of candidates, some with more potential than others for large scale use. Examples include the addition of; carbon nano-tubes,[3] ionic stabilisers,[4] polymers,[5] geo-polymers,[6] lignosulfonates,[7] enzymes,[7] microbially induced precipitation,[8] biopolymers,[9] fungal hyphea,[10] and surface modification agents.[11]

Enhancements in soil strength have been achieved with these non-traditional additives, however some limitations have prevented their large-scale implementation. Reasons include the use of potentially environmental toxic precursors (polymers, geopolymers, surface modification agents) and the inhospitality of certain soil types, such as mine tailings, to biotic based additives (microbially induced precipitation, fungal hyphae).

The use of biopolymer additives however, is a promising avenue. Advantageous characteristics include; abiotic, aqueous solubility, low energy preparations, low cost, low additive quantity required, high strength and CO_2 negative production. Potential disadvantages include the loss of strength under saturation and a vulnerability to microbial degradation.[12]

Previous investigations have demonstrated biopolymer additives can achieve an unconfined compressive strength (UCS) that exceeds cement stabilised soils (a measure often used to determine stabilization/solidification potential). Chang *et al.*[13] used 1% ($Mass_{additive}$ / $Mass_{material}$) Xanthan Gum, a microbially produced biopolymer, resulting in an 86% increase in UCS compared to 10% cement addition to soil material. Muguda et al.[14] identified a 30% higher UCS using 3% Guar Gum, (a plant derived biopolymer additive), compared to 8% cement addition. The ability of biopolymers to sustainably stabilize/solidify soil material is attracting a growing amount of civil engineering research.

One of the major challenges in exploiting biopolymer additives is that geotechnical lab testing is often labor intensive, requires high resource investment, and is frequently based upon trial and error investigation. The field would benefit from development of high throughput, scientific, systematic approaches to study how biopolymer additives interact with geomaterials so that their strengthening properties can be understood, developed and tuned for a particular soil system, before scaling up to intensive geotechnical laboratory and field testing.

Within this study we demonstrate the power of using a Membrane Enabled Bio-Mineral Affinity Screen (MEBAS), for the high throughput identification of strong biopolymer-mineral composites, before Geotechnical Verification (GV) lab testing (Figure 1). Previous investigations have shown the versatility of membrane based dot blot screening to identify interactions in a range of systems including; peptides-bacteria,[15] peptide-particular matter (elemental & organic carbon)[16] and peptide – nanoparticles (e.g. Au).[17] Although membrane

immobilization of non-protein biopolymers has been previously achieved,[18] to the knowledge of the authors, this is the first study to extend the use of membrane assays to screen for biopolymer – geomaterial interactions.

We then outline a secondary Mineral Binding Characterization (MBC) step to further elucidate the binding mechanisms associated with high affinity bio–mineral composites at the molecular level.
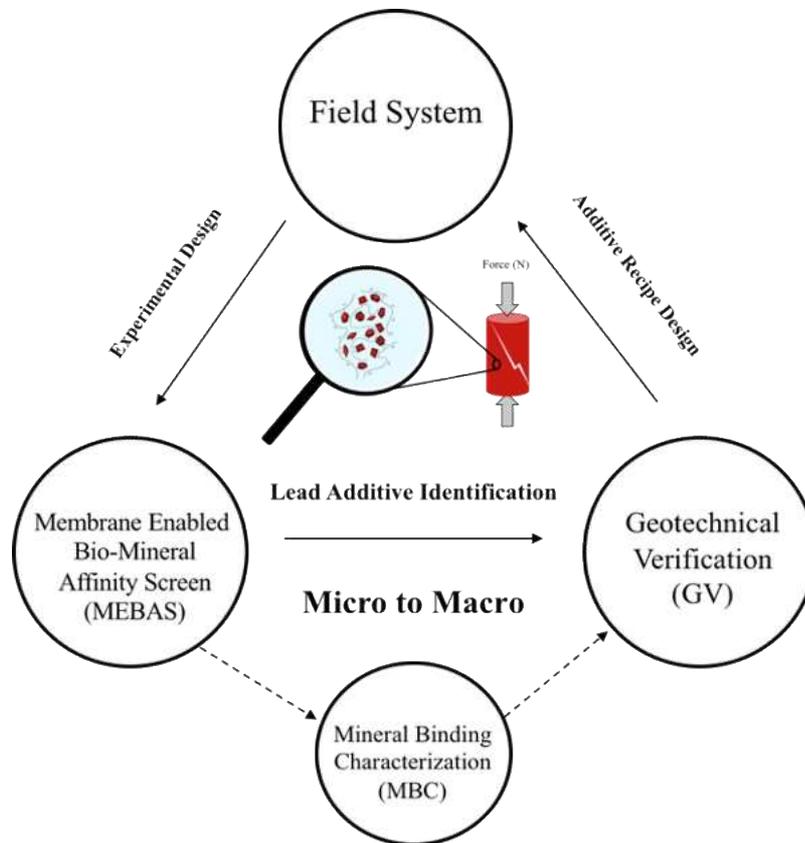
Figure 1. A schematic representing a cross-disciplinary, micro-macro approach to determine additive recipes for the stabilization/solidification of soil systems. Field systems are first investigated to determine experimental material properties. A simple, high throughput, MEBAS is then carried out upon the selected mineral in order to determine lead biopolymer additives for up-scale investigations. Geotechnical Verification (GV) is then performed to confirm superior stabilization/solidification. This process allows for the quick design of sustainable additive solutions for stabilization/solidification. A secondary step using Mineral Binding Characterization (MBC) is further outlined to both confirm binding observed via MEBAS and also understand the binding mechanism associated with high affinity bio-mineral interactions. This step provides information towards the mechanisms underlying those observed in the upscaled GV tests.

Mine Tailing (MT) geotechnical structures are adopted as an exemplar application for this study. A significant proportion of mine waste is stored using tailing dam facilities. Current yearly production of mine waste exceeds 100 billion tonnes.[19] Due to increasing mineral demands and grade ore quality falling (as high-grade ores are depleted), this number is expected to exponentially rise.[20] At least one major tailings dam disaster occurs each year, for example

in 2019 a failure in Brumadinho, Brazil resulted in the release of 11.7 million m^3 of mining mud, causing at least 220 deaths and devastating environmental damage to over 600km of the Rio Paraopeba.[21, 22] Stabilization/solidification is a key MT disaster mitigation strategy.

A simplified MT system based on iron-oxides has been selected due to its universal abundance (Figure S1) and more reactive chemistry, making it an important candidate for biopolymer additive binding.[23] Surprisingly there is very little literature with respect to utilization of iron minerals for stabilization/solidification.

Although MT systems often comprise a high proportion of gangue SiO_2 material (Figure S1), previous literature has reported the lack of direct chemical interaction between biopolymers and the SiO_2 mineral surface.[24, 25] This study therefore aims to demonstrate the power of the proposed rapid, micro-macro, MEBAS-MBC-GV framework for the identification and understanding of biopolymer stabilization/solidification additive recipes, utilizing the iron-oxide component of an MT system as an exemplar application.

2. EXPERIMENTAL DESIGN AND SAMPLE PREPARATION

2.1. MT Exemplar Experimental Parameters. SiO_2 was the major constituent (50-82%) in all of the literature sampled MTs (Figure S1). Iron oxide content was found to be the next most common constituent with Fe_2O_3 comprising 10.91% +/-3.4%. Al_2O_3 and CaO components were disregarded from the exemplar MT system as they are in smaller and inconsistent quantities across the MT available literature and to maintain simplicity in the model system. Typical MT materials exhibit high proportions of silt (2-63 μm) and very-fine sand (63-125 μm). Gorakhi et al.[26] provided examples of typical MT particle size distribution curves.

In order to probe the bio-mineral interface a simplified artificial MT exemplar was adopted, comprising 90% relatively bio-minerally inactive SiO_2, and 10% Fe_2O_3. The red color of Fe_2O_3 (Hematite) particles renders them ideal for visualization against the white Nitrocellulose membranes used in this study. The particle size of both components (SiO_2 = 90-150μm, Fe_2O_3 = 224nm +/- 119nm) was selected to match the data available for real MT samples. This simplified system allows for controlled investigation of the bio-mineral interface within a defined set up.

The pH of fresh MT is typically between pH 7-8 (Figure S1). As a result, pH 7 was selected for the 'macroscopic' studies, as it is critical that there is strength at this pH. For initial high throughput 'microscopic' studies a pH range of 4-8 has been selected. This is to account for the likelihood of acid generation by oxidizing minerals, resulting in the importance that strength is not lost at a lower pH as the MT ages.

2.2. Biopolymer Experimental Parameters. Cornell et al.[27] highlighted the ability of ligands within biomolecules, to act as multi-site coordination complexes forming bridges between iron particles. Polysaccharides in particular can facilitate this process at metal oxide surfaces through acid-base reactions, and were therefore selected as the focus for this study. Locust Bean Gum (LB), Guar Gum (GG), Xanthan Gum (XG), Sodium Carboxy Methyl Cellulose (CMC) and High Acyl Gellan Gum (Ge) were selected due to their differing chemical characteristics (Figure S2).

Through preliminary results an optimum initial water content of 27.5% ($Mass_{water}$/$Mass_{sand}$) has been determined (Figure S3). Initial experiments using GG (Figure S4). determined 1%

($Mass_{biopolymer}/Mass_{sand}$) as the optimum additive addition quantity. In order to compare Fe_2O_3 binding potential, molarity (0.2M, determined from GG) has been used to ascertain LB, XG, CMC and Ge addition quantities. Biopolymer molar masses were determined via average sugar monomer molecular weight (Figure S5).

Through preliminary investigation suitable additive preparation conditions utilizing a moderate temperature (40℃, 10 minutes) whilst simultaneously stirring (300 rpm), followed by ultra-sonication (10 minutes) was determined (Figure S4). This methodology was used to avoid higher temperature, energy intensive preparation conditions typically used within the literature (Figure S6).

3. MATERIAL AND METHODS

3.1. Materials and Reagents. Reagent-grade chemicals; Locust Bean Gum (LB), Guar Gum (GG), Xanthan Gum (XG), Gellan Gum (Ge), Sodium Carboxymethyl Cellulose (CMC), were purchased from Sigma Aldrich/Merck and used without further purification. Fe_2O_3 was acquired from Mineral Waters Ltd and used as supplied. Amersham^{TM} Protran^{TM} $0.2\mu m$ Nitrocellulose Blotting Membrane was purchased from GE Healthcare Life science. SiO_2 Fraction E (90-150μm) was purchased from David Ball sand specialists.

3.2. Biopolymer additive solution preparation. All biopolymer additive solutions were prepared using the same methodology. Biopolymer average monomer molecular weight was used to achieve a target concentration. Powdered biopolymer was first added to a temperature controlled (40°C) ultra-pure water solution whilst simultaneously agitating with a magnetic stirrer (GV 300 rpm, MEBAS-MBC 600 rpm). Solutions were then incubated (10 minutes, 40°C) and subsequently sonicated (10 minutes) using a VWR Ultrasonic water bath. Once prepared, solutions were stored in darkness and used within 24 hours of preparation.

3.3. Membrane Enabled Bio-Mineral Affinity Screening (MEBAS). MEBAS was carried out using nitrocellulose (0.2μm pore size) membranes. 5μl of each prepared biopolymer solution (0.04M) was arrayed onto a nitrocellulose membrane in triplicate (Figure S7, A). After air drying, the membrane was submerged in a 3% wt/vol bovine serum albumin solution for 1 h to saturate any available nitrocellulose not covered by the arrayed biopolymers. The membrane was then washed with ultrapure water before being subjected to an EDTA 10mM wash for 1h to ensure any bound metal cations are removed.

Membranes were then subjected to a final wash (5 times, 2 mins) with an aqueous solution characteristic of the conditions used for the subsequent binding experiment (over a pH range of 4-8). All pH adjustments were made using NH_4OH (0.5M)/HCl (0.5M). Fe_2O_3 (3 mg) particles were added to ultra-pure water (35ml) and the pH adjusted to the desired value. Fe_2O_3 suspensions were then sonicated (2 minutes, 8 kHz, 50:10 impulses). The prepared membrane was then submerged in the suspension (Figure S7, B) for 4 h whilst mixing. The membranes were then washed twice for 10 minutes using pH adjusted ultra-pure water. A Chemi-Doc gel documentation system (Bio-Rad, UK) was used to visualize and photograph the membranes and quantify the Fe_2O_3 screening intensities (Figure, S7, C) via densitometry.

3.4. Fe_2O_3 Particle Characterisation. Power XRD patterns of dry Fe_2O_3 particles were collected using a standard X-ray diffractometer with Bragg–Brentano geometry (Bruker D8, CuKα radiation, $\lambda = 1.54178$ Å). Scattering angle 2θ was scanned in a range of 20–70° at 0.022° increments.

A Tecnai T12 Spirit Transmission Electron Microscope, equipped with a camera, was used to image Fe_2O_3 particles. Samples were prepared by dropping $10 \mu L$ of 1mg/mL Fe_2O_3 suspension onto a carbon coated, copper, TEM grid. The grid was then left to dry for 1 hour before imaging. TEM images were analysed using Image-J software (v1.52 a, public domain, National Institute of Health, Md, USA). 200 particles were randomly selected and measured to determine a particle size distribution.

3.5. Mineral Binding Characterization (MBC). 0.01 M solutions of each biopolymer were prepared in ultra-pure water. Fe_2O_3 (64 mg, 0.02M) particles were then added and dispersed via sonication (10mins, VWR Ultrasonic water bath). The solution pH was then adjusted to pH 7 using NH_4OH (0.5M)/HCl (0.5M) where necessary. The solutions were then rotated for 30 minutes using a Lab net Mini Labroller^{TM}. Biopolymer coated particles were separated using centrifugation (4000rpm, 10 mins) and washed using ultra-pure water to remove excess non-bound biopolymers (4 repeats). Particles were then left to dry at room temperature, ready for analysis.

Particle organic coating masses were determined using a PerkinElmer Pyris 1 Thermal Gravimetric Analyzer (TGA). Dry Bio-Fe_2O_3 particles were exposed to a temperature range of 20-800℃ under a 2/3 N_2, 1/3 O_2 atmosphere. Biopolymer mass loss (%) was determined between 200-400℃.

Surface functional groups were determined using a Perker Elmer Frontier Fourier Transform Infrared (FTIR) and Golden Gate Diamond Attenuated Total Reflection (ATR) spectrometer. Data collection and analysis was performed using Spectrum^{TM} 10. Scans were made between 4000cm^{-1} and 400 cm^{-1}. Baseline correction was performed on all spectra.

Zeta potentials were determined using a Brookhaven BI-900AT. Bio-Fe_2O_3 particles were ground using a pestle and mortar and dispersed (0.01 g/ml) via sonication (10 minutes, VWR Ultrasonic water bath) in a KNO_3 (10 mM) solution. The solution pH was adjusted using NaOH (0.5M)/ HCl (0.5M) to pH 7. Samples were scanned 5 times at 25℃ and data analysed using Malvern ZetaPlus software.

3.6. Biopolymer Circular Dichroism. Circular dichroism is technique utilizing circularly polarized light to determine structural information about biomolecules, such as the polysaccharides used within this study. A Jasco J-810 instrument was used to collect CD spectra. Biopolymer solutions were prepared to a concentration of 0.04 M. Serial dilutions were then carried out using ultra-pure water to achieve concentrations 0.02, 0.01, 0.005, 0.0025M. The biopolymer solution was then transferred to a cuvette with a 2mm pathlength. The wavelength was scanned between 190-220nm with a 1nm slit width at 1s intervals at 20℃. Scans were repeated 4 times per sample, the results averaged, and an aqueous baseline subtracted.

3.7. Geotechnical Verification (GV). SiO_2 fraction E (144g, 90-150μm) was first mixed with Fe_2O_3 (16g, 224nm +/- 119nm) to achieve a simplified tailings equivalent synthetic material. Powdered biopolymer was added to 44ml (27.5%, Mass$_{water}$/Mass$_{sand}$) of ultra-pure water, following the biopolymer solution preparation procedure previous outlined, to achieve a concentration of 0.2 M +/- 0.02 M. Solutions were then immediately mixed through 160g of material until a homogenous mix was achieved.

The resulting composite was then divided into 3 equal parts and compacted using a cylindrical drop hammer (2.1103 Kg, 246 mm × 37 mm) via 10, 126 mm drops, within a 202 mm × 42 mm hollow cylindrical sample mold. Samples were then extruded and left to cure for 7 days at 20℃. All sample series (Fe and non Fe systems) were prepared and cured at the same time to ensure identical curing conditions. The 7 day sample moisture contents were closely similar for all biopolymer treated samples at 9-11% (Figure S8). A digital Tri-test ELE was then used to perform unconfined compressional strength tests following the ASTM D2166 standard method.[28] A rate of displacement of 1.5mm min^{-1} was utilized throughout all testing. Load (N) and displacement (mm) data were collected during tri-axial tests. The UCS (kPa) at failure of each sample was determined as the peak applied axial load (N), per cross sectional area. Further to unconfined compressive strength tests at 7 days, samples were fully submerged within ultra-pure water for 24 hours to qualitatively determine the effects of aqueous saturation.

4. RESULTS

4.1. Fe_2O_3 Particle Characterization. Fe_2O_3 particles were characterized using XRD, TEM, ATR-FTIR and Zeta potential and the particle size distribution determined (Figure S9).
All analyses indicated the presence of α-Fe_2O_3 with a size distribution of 224nm +/- 119nm (Mean +/- SD), and without any significant contamination of alternative iron oxide phases.[29, 30, 31]

4.2. MEBAS: Biopolymer-Fe_2O_3 Affinity between MT relevant pH (4-8) range. All additives were spotted in triplicate onto a membrane and Fe_2O_3 particles were introduced to rapidly screen their binding propensity (Figure 2).

Overall LB, GG, XG and CMC all showed Fe_2O_3 binding affinities within the MT relevant pH range (4-8), peaking at pH 4 (Figure 2, A). Ge showed no binding throughout the full pH range. At neutral pH 7, LB and GG (neutral polyols) exhibit a significantly higher affinity than the other 3 additives (Figure 2, B). This is important as pH 7 is the relevant pH for freshly extracted MT's. It is beneficial that binding intensity increases upon a decrease in pH, which may occur as aging MT acidify, improving Fe_2O_3 binding affinity over time.

XG and CMC (anionic polyelectrolytes) showed a low binding affinity through the neutral pH range (5-8) indicating their unsuitability for use as MT stabilization/solidification additives in fresh tailings. However, within acidic conditions (pH 4) both additives show Fe_2O_3 binding (Figure 2, A).
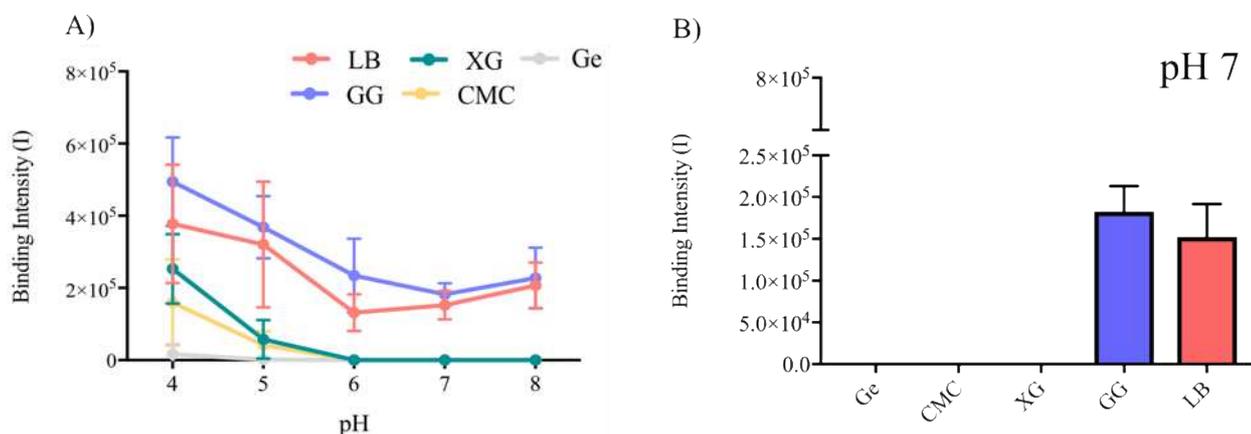
Figure 2. MEBAS analysis. A) Graph showing biopolymer-Fe_2O_3 binding intensities through mine tailing's relevant pH range (4-8). B) Graph showing binding intensity of biopolymer (0.004M) - Fe_2O_3 (0.06mg/ml) affinity at pH 7. Binding intensities were determined via the subtraction of a local control background reading. Membrane images are displayed in figure S10.

4.3. MBC: Thermal Gravimetric Analysis (TGA) of Biopolymer Coated Fe_2O_3 Particles.
TGA can be used to determine the quantity of organic coating on a mineral particle. All mass loss occurred between 200-400°C (Figure S11) which indicates the combustion of organic surface species. This can be directly attributed to the amount of biopolymer bound to the Fe_2O_3 surface.[32, 33]

At pH 7 (Figure 3, A), Fe control (no coating) Ge, CMC and XG exhibited a negligible mass loss of 0.87%. 0.69%, 0.39% and 0.27% respectively. LB and GG produced significantly larger mass loss of 8.6% and 4.5% respectively. These results confirm the findings from the screening experiment, and identify LB and GG as lead biopolymers for further analysis.

4.4. MBC: Zeta Potential of Biopolymer Coated Fe_2O_3 particles. Zeta potential is a technique used to characterize surface charge at the solid/liquid interface. It is often used to determine the surface charge of metal oxides as a function of pH.

LB-Fe_2O_3 and GG-Fe_2O_3 show zeta potentials of -9.72 and -11.36 respectively (Figure 3, B). The significant reduction in negative surface charge relative to Fe_2O_3 control particles (-24.31 mV) is attributed to the presence of LB/GG biopolymer surface coating. LB and GG exhibit a similar surface charge which suggests a similar type of coating. The surface charge for both LB/GG-Fe_2O_3 particles is within the 'threshold for aggregation'[34] (+/- 15), meaning aggregation between bio-Fe_2O_3 particles is likely to occur. This could explain the formation of visible aggregates during LB/GG-Fe_2O_3 particle preparations.

XG, CMC and Ge treated Fe_2O_3 particles all show small changes in surface charge to -30.10mv, -32.21mv, and -28.18mv respectively (Figure 3, B). These shifts suggest a very small quantity of biopolymer is present on the Fe_2O_3 surface

4.5. MBC: ATR FTIR of Biopolymer Coated Fe_2O_3 particles. Attenuated Total Reflectance Fourier Transform InfraRed spectroscopy (ATR-FTIR) was used to probe the chemical interactions associated with the adsorption of organic molecules at the bio-mineral interface.[35]

The Fe_2O_3 control, LB-Fe_2O_3 and GG-Fe_2O_3 samples all produced peaks at 433 cm^{-1} and 518 cm^{-1}, consistent with the Fe-O bonds of Fe_2O_3 (Figure 3, C).[30] LB and GG produced peaks at 873 cm^{-1} and 811 cm^{-1} corresponding to the anomeric C-H groups of galactose and mannose respectively. Within the OH bending region (1200-780cm^{-1}) Fe_2O_3 peaks are found at 914 cm^{-1} and 1155 cm^{-1}(Figure 3, C), which are attributed to Fe-OH surface groups[31]. LB and GG control spectra both exhibit; C-O-C$_{bend}$ at 1146 cm^{-1} and 1142 cm^{-1} , Galactose C-OH$_{bend}$ at 1054 cm^{-1} and 1062 cm^{-1} and Mannose C-OH$_{bend}$ at 1015 cm^{-1}, and 1016 cm^{-1}.[36]

Upon equilibrating with Fe_2O_3, both LB and GG C-OH$_{stretch}$ and C-OH$_{bend}$ peaks shift to a higher wavenumber and a loss in absorption intensity is seen (Figure 3, C). This is attributed to the loss of C-OH groups due to the formation of C-O-Fe at the Fe_2O_3 surface. No change in surface spectra was seen for XG, CMC and Ge coated Fe_2O_3 particles (Figure S12).

Figure 3. MBC analysis of Bio-Fe_2O_3 (0.01M:0.02M) particles at pH 7. A) TGA of Bio-Fe_2O_3
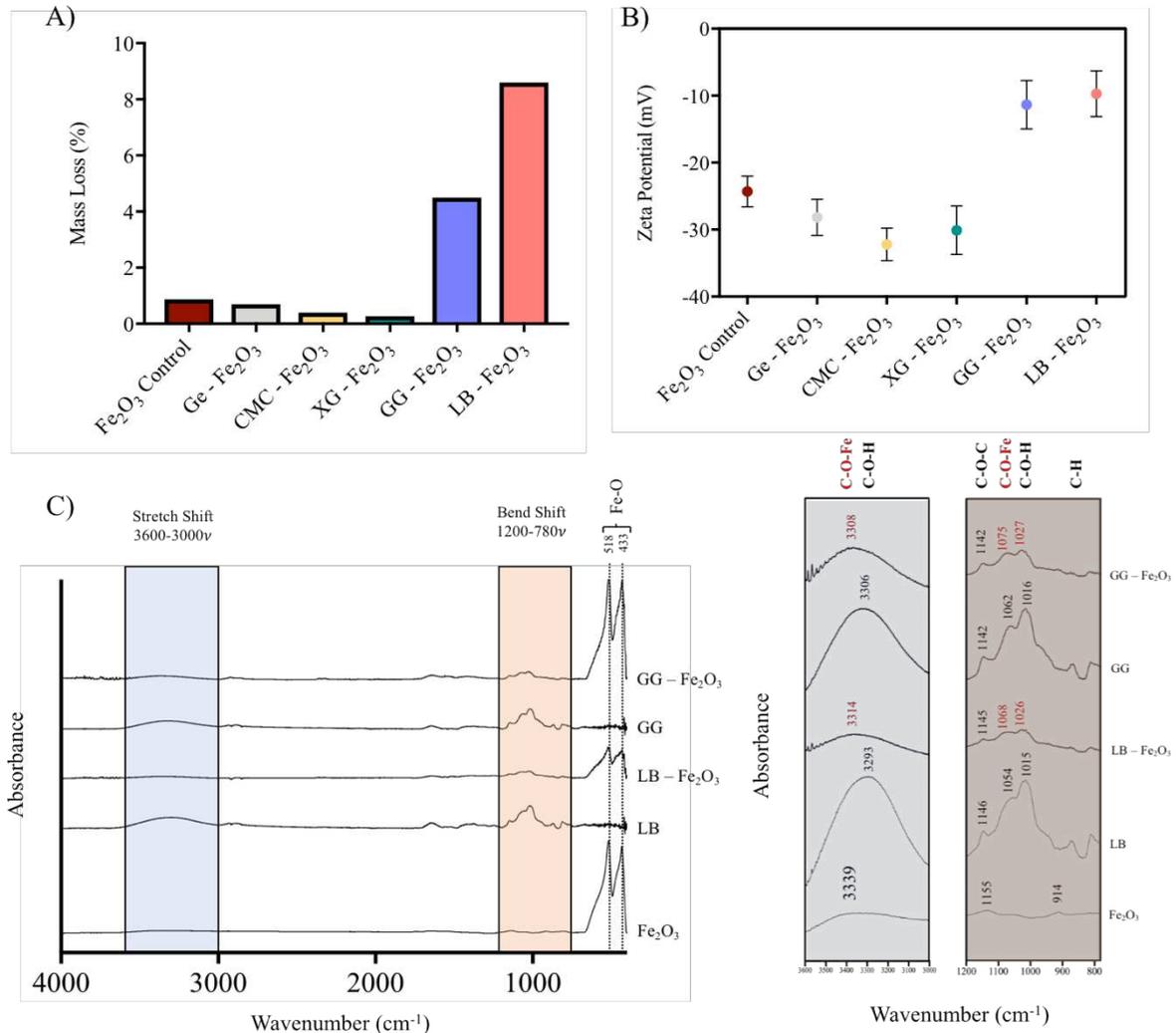
particles. Mass loss (% of total mass) upon a temperature gradient (200-400°C). B) Zeta potential (mV) of Bio-Fe_2O_3 particles (0.01mg/ml) dispersed within a KNO_3 (10mM) solution at pH 7. C) ATR-FTIR of Fe_2O_3 control, LB control, LB-Fe_2O_3, GG Control and GG-Fe_2O_3 particles. Major Fe-O peaks (433, 518), stretch (3600-3000υ) and bend regions (1200-780υ) have been identified and labelled. Major shifts in wavenumber (υ) peak shifts and absorption intensity have been highlighted.

4.6. GV: Biopolymer Stabilization/Solidification Characteristics. Due to the cementation induced by biopolymer addition, testing was performed using an unconfined compression test (UCS) typically used for stabilised/solidified soils.

Qureshi et al.[37] found the addition of 10% cement to SiO_2 sand ($D_{90} = 200\mu$m) achieved a UCS of 1767 kPa after 7 days curing, and was used as a comparison in this study. Upon the addition of biopolymer additive (0.2M +/- 0.02M) to control SiO_2 (100%) samples, (Figure 4,
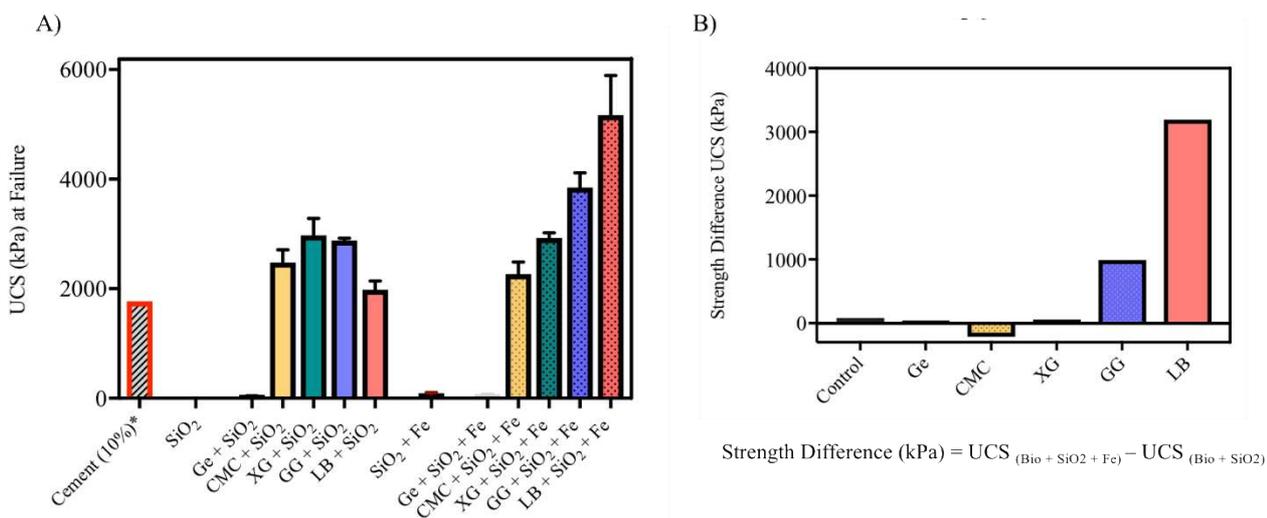
A) a UCS (after 7 days curing at 20℃) of; CMC (2475 kPa), XG (2975 kPa), GG (2878 kPa) and LB (1979 kPa) was achieved. A negligible UCS was observed for Ge (35 kPa) stabilised samples.

The same test was then conducted on the exemplar MT system of 90% SiO_2 and 10% Fe_2O_3. LB and GG improved the UCS of the MT system remarkably, with values of 5171 kPa and 3848 kPa respectively, a significant improvement over biopolymer stabilised SiO_2 (100%) samples (Figure 4, B). The addition of biopolymer additives to the MT system resulted in UCS of CMC (2261 kPa), XG (2925 kPa) and Ge (54 kPa), a non-significant change in strength characteristics compared to biopolymer stabilised SiO_2 (100%) samples. The addition of Fe_2O_3 (10%) resulted in a small increase in UCS (83kPa) when compared to SiO_2 (100%) control samples, however both control samples exhibited weak strength characteristics. The low UCS (kPa) achieved for control samples and comparable moisture content retention (day 7) exhibited by biopolymer stabilized samples demonstrated that water-mineral capillary suction effects were comparatively negligible in this study (Figure S8).

Figure 4. Summary graph of UCS at failure and strength increase upon the addition of Fe_2O_3 (10%). A) UCS (kPa) of biopolymer (0.2M, 27.5% $Mass_{water}/Mass_{solution}$) stabilised samples determined following 7 days of curing at 20℃. The UCS of a cement (10%) stabilised equivalent system is presented.[84] SiO_2 (100%) systems are labeled as biopolymer additive + SiO_2. SiO_2 (90%) + Fe_2O_3 (10%) samples are labeled as SiO_2 + Fe. B) UCS (kPa) difference between biopolymer additive (0.202M, 27.5% ($Mass_{water}/Mass_{solution}$) stabilised SiO_2 (100%) and SiO_2 (90%) + Fe_2O_3 (10%) artificial MT samples.

5. DISCUSSION

First we discuss the use of the MEBAS-MBC-GV framework within the context of a simplified MT exemplar system, outlining the understanding it provides. The implications of biopolymer-mineral interactions on both the micro and macroscopic properties are then outlined. Finally we discuss the individual MEBAS-MBC techniques and their potential use for future studies.

5.1. Biopolymer Stabilization/Solidification of a SiO_2 (100%) system.
Stabilization/solidification was first carried out in a simple, SiO_2 (100%) system to determine baseline biopolymer strength implications. Upon the addition of 0.2M (~ 1%,

12

Mass$_{biopolymer}$/Mass$_{sand}$) biopolymer additive to SiO$_2$ (100%), not only was there a significant increase in strength relative to the negligible UCS exhibited by SiO$_2$ alone, but for all biopolymers (except Ge) the strength exceeded the UCS achieved by an 10% cement mixture.

Although the focus of this paper was the study of the more reactive Fe$_2$O$_3$ mineral surfaces, it is useful to consider the interactions occurring in the biopolymer-SiO$_2$ controls. The UCS improvements seen within SiO$_2$ (100%) systems upon biopolymer addition are attributed to electrostatic adsorption of biopolymer additives to negatively charged SiO$_2$ surfaces, facilitated by aqueous molecules (Figure S13, A, C).[38, 39] The inability of biopolymers to form direct interactions with the SiO$_2$ surface is attributed to strong interfacial aqueous interactions at the SiO$_2$ surface.[40] The non-specificity of the electrostatic and hydrogen bonding explains why a similar UCS improvement is seen with CMC, XG and GG ($\sim$ 2725 kPa $\pm$ 250 kPa). These biopolymer additives contain primarily hydrophilic groups which can participate in aqueous mediated electrostatic interactions. LB however exhibits a lower UCS. This is attributed to the high proportion of exposed hydrophobic β-(1-4)-D-Mannan groups on the LB backbone. These groups are more likely to bind to one another to minimise aqueous interactions. This highlights the interplay between hydrophilic/hydrophobic and electron double layer interactions, which needs close consideration when selecting biopolymers for stabilization/solidification.

5.2 XG and CMC Biopolymer Stabilization/Solidification of a MT Exemplar System. Due to its universal abundance within MT and higher surface reactivity (relative to SiO$_2$) a Fe$_2$O$_3$ based MT exemplar system (SiO$_2$ 90%, Fe$_2$O$_3$ 10%) has been investigated. Fe$_2$O$_3$ was first taken through the MEBAS-MBC framework to both identify lead biopolymer stabilization/ solidification additives and to understand their mineral binding mechanisms before GV.

Throughout the MEBAS-MBC investigations, XG and CMC biopolymer additives show a negligible binding interaction for Fe$_2$O$_3$ particles at pH 7. XG and CMC's pKa is 3.1 and 3.6 respectively.[41, 42] Therefore, within neutral conditions (pH > pKa) carboxyl side chains are deprotonated. This produces negatively charged groups along the polymer side chains. Fe$_2$O$_3$ particles exhibit negative surface charges (-24.31mv) at pH 7. Therefore, the lack of Fe$_2$O$_3$ binding in the MEBAS-MBC investigations could be attributed to repulsion between negatively charged mineral surface groups and negatively charged biopolymer additive side chains. At pH 4 XG and CMC both exhibit Fe$_2$O$_3$ binding within MEBAS. This can be ascribed to protonation of the XG and CMC side chains, reducing negative charged repulsions at the bio-mineral interface. This highlights the importance of pH in bio-mineral interactions. MT systems often vary in pH over time and space due to the oxidization of minerals.[43] MEBAS has the advantage of allowing the high throughput, simultaneous screening of multiple bio-mineral interactions at different pH conditions.

Within the GV investigations, upon the addition of XG and CMC to exemplar MT material no significant change in UCS relative to the SiO$_2$ stabilised samples (Figure 4) is seen. This is attributed to both Fe$_2$O$_3$ and SiO$_2$ having a negative surface charge of -24.31mv and -47mv[44] respectively, resulting in the biopolymers' ability to interact through the same aqueously mediated, electrostatic coordination mechanism with both surfaces (Figure S13, C). The small amount of biopolymer observed on the iron-oxide surface with TGA analysis and no change in surface bonding seen within ATR-FTIR spectra (Figure S12, A, B) supports this hypothesis.

5.3 Ge Biopolymer Stabilization/Solidification of MT Exemplar System. Upon the addition

of Ge to geotechnical samples, substantially lower UCS values are achieved relative to other biopolymers. Furthermore, although it is poly-anionic with a pKa 3.6, unlike CMC and XG, it does not bind Fe_2O_3 at pH 4 during MEBAS.[45] Ge however is the only biopolymer additive within this study which is known to produce a sol-gel transition without the further addition of reagents (Figure S14, A, B).[46] Gelation has been observed using Circular Dichroism (Figure S14, B). It is hypothesized that upon gelation intra-molecular interactions shield biopolymer functional groups, rendering them unavailable for Fe_2O_3 binding. Particles are thus suspended (not bound) within the biopolymer gelatinous matrix which becomes the basis of the strength characteristics (Figure S13, B). This shows the power of utilizing the MEBAS-MBC-GV framework to understand, hypothesize and investigate biopolymer stabilization/solidification additives. Furthermore, the potential limitations of gel forming biopolymer additives are highlighted.

5.4. LB and GG Biopolymer Stabilization/Solidification of MT Exemplar System. Relative to biopolymer stabilised SiO_2 (100%) samples, the highest increase in UCS for the exemplar MT material (with the addition of 10% Fe_2O_3) achieved during GV was found with LB (3192 kPa) and GG (991 kPa) (Figure 4, B). The resulting UCS of 5171 kPa and 3848 kPa give a 293% and 218% increase in strength compared to that achieved by a 10% cement addition. This increase in strength highlights the power of identifying strong bio-mineral composites through MEBAS and also further emphasises that not only do biopolymers exhibit desirable environmental characteristics but also an improved stabilization performance, at much lower concentrations, when compared to cement stabilization/solidification of soils.

Through MBC it is clear that binding of LB and GG changes the Fe_2O_3 particles surface functionality. The presence of shifted biopolymer O-H$_{stretch}$, C-OH$_{bend}$ and C-O$_{bend}$ peaks within the Bio-Fe_2O_3 FTIR, signifies the involvement of these groups within the bio-mineral interaction. We hypothesize that β-(1-4)-D-Mannan groups, which are unable to form aqueously mediated electrostatic interactions with SiO_2 particles due to their hydrophobicity, when exposed to Fe_2O_3 particles, are able to form specific covalent interactions through acid/base reactions, forming C-O-Fe bonds. A shift in surface charge to within the 'threshold of aggregation' (-15mv) indicates a further electrostatic contribution to the binding interaction. Therefore, it is proposed that LB and GG form a matrix with the Fe_2O_3 particles through a combination of specific covalent and non-specific electrostatic interactions (Figure S13, A), increasing the macroscopic stabilization/solidification effect. This agrees with previous hypothesized GG-Fe_2O_3 binding models.[47, 48]

5.5. Effect of LB/GG-Fe_2O_3 interactions upon Biopolymer Stabilization/Solidification disadvantages. A common pitfall with previous biopolymer stabilization examples is their tendency to disintegrate following submersion in water, reducing the scope of their applications[12]. Since the current MEBAS experiments are performed under saturation, this provides indications about which bio-mineral interactions outcompete bio-water and mineral-water interactions. In our case, when submerging LB stabilized SiO_2 (100%), a loss in sample structural integrity was observed (Figure S15, B). This is attributed to the extension of the electron double layer under saturation, resulting in the reduction of electrostatic and hydrogen bond bio-mineral interactions previously outlined (**5.1**).[49] In contrast, upon the addition of LB to Fe_2O_3-SiO_2 mixtures, better retention of sample structural integrity was seen (Figure S15,

A). This is tentatively ascribed to the resistance of the specific polymer-mineral interactions to rehydration, and is an area requiring further study.

A further concern associated with the use of biopolymers as stabilization/solidification additives is their vulnerability to microbial attack. However a recent study by Landlorde et al.[50] found that 21% $\pm$ 8.6% of organic carbon within sediments are associated with reactive iron phases. Further investigation by Barber et al.[51] found that this phenomena was driven by the formation of irreversible covalent C-O-Fe complexes, such as LB/GG-Fe_2O_3 interactions found within this study, which reduce both the biopolymer enzymatic hydrolysis and biodegradation. The implications of this phenomena upon LB/GG degradation and its implication on long term stabilization/ solidification potential are additional promising areas for further study.

5.6. Utilizing MEBAS-MBC-GV framework for the development of Biopolymer Stabilization/Solidification additive recipes. This study has demonstrated the successful utilization of a micro-macro, MEBAS-MBC-GV framework for the identification and understanding of biopolymer stabilization/solidification additives for a MT exemplar system. It is worth however discussing the use of individual MEBAS-MBC-GV methodologies.

Similar trends are seen between the microscopic MEBAS and macroscopic TGA results, however, the correlation between the microscopic TGA and macroscopic GV results are remarkably aligned. This is to be expected when one considers that the materials used in both the GV and TGA are in more similar environments (biopolymer coated Fe2O3 particles), whereas the MEBAS results are obtained from particles interacting with a 2D biopolymer surface. However, when considering the results per day between MEBAS (36 – with potential for scale up) and GV (0.75), MBC:TGA (2) and MBC:ATR-FTIR/Zeta Potential (2) the capacity of MEBAS as a high throughput tool for quick identification of strong bio-mineral composites is highlighted (Figure S16) and was estimated to provide an approximate 50-fold increase in the rate of assessment compared to GV alone in this study.

It is worth noting that MEBAS-GV on its own has the ability to identify lead biopolymer stabilization/solidification additives. The MBC step should be employed when a greater understanding is either required or desired and when the suitable chemical analytic equipment is available.

5.7. Future Use of the MEBAS-MBC-GV framework. This study has shown that 'microscopic' high throughput analysis can predict significant 'macroscopic' improvements in physical characteristics . By using this framework, a 293% and 218% increase in the failure strength over an 10% cement addition has been demonstrated for just 1% LB and GG addition respectively. This increase highlights the power of identifying strong bio-mineral composites as superior sustainable alternatives to e.g. cement stabilization/solidification of soils. Furthermore, through MBC the significance of biopolymer functional groups, mineral surface charge and reactivity has been highlighted. This has allowed the development of bio-mineral binding models for a MT exemplar system, highlighting, for example, LB/GG's ability to form strong bio-mineral interactions through a combination of covalent C-O-Fe bonds and non-specific electrostatic biopolymer-SiO_2 interactions.

It should be possible to extend MEBAS to screen a vast catalogue of biopolymer additives against mineral and ion components across a full range of conditions such as temperature, pH, electrical conductivity and aerobic/anaerobic conditions typically found within soil systems, to produce specialised biopolymer additive 'recipes'. Additionally, variables can be screened

concurrently to replicate more complex 'real world' systems. It is worth noting that in order to screen light colored minerals such as Al_2O_3 (Kaolin) and CaO ($CaCO_3$) it would be important to select a contrasting membrane color to allow for MEBAS imaging and quantification steps. A MBC step can then further be utilized to decode interactions to build an understanding about the driving mechanisms associated with strong bio-mineral interactions.

In summary, it is anticipated that the proposed framework will contribute to the provision of an efficient, systematic methodology in selecting lead biopolymer candidates for the design of new sustainable geotechnical solutions.

ACKNOWLEDGEMENTS

SUPPORTING INFORMATION

The Supporting Information contains 16 figures (Figure S1-S16).

Typical Mine Tailing ore, mineral composition and pH (Figure S1); LB, GG, XG, Ge, CMC biopolymer characteristics (Figure S2); UCS of LB & GG stabilised samples upon a variation in initial moisture content (Figure S3); UCS of GG stabilised samples upon a variation in additive solution preparation conditions and curing times (Figure S4); Example method to determine biopolymer average monomer molecular weight (Figure S5); Typical biopolymer additive solution preparation conditions (Figure S6); Schematic showing MEBAS methodology used to quantify bio-mineral interactions (Figure S7); Moisture Content Retention (%) of biopolymer stabilized samples (Figure S8); Fe_2O_3 particle characterization (Figure S9); Chemi Doc membrane images post Fe_2O_3 MEBAS experiments (Figure S10); Individual bio-Fe_2O_3 TGA curves (Figure S11); XG, CMC and Ge bio-Fe_2O_3 ATR-FTIR (Figure S12); Schematic showing bio-mineral binding models determined via the MEBAS-MBC framework (Figure S13); Circular dichroism of Ge biopolymer solutions (Figure S14); Qualitative analysis of LB stabilised samples strength under saturation (Figure S15); Table highlighting expected 'results per day' using individual MEBAS-MBC-GV techniques. (Figure S16) (PDF).

REFERENCES

(1)   Manjunatha, L. S.; Sunil, B. M. Stabilization/Solidification of Iron Ore Mine Tailings Using Cement, Lime and Fly Ash. *Int. J. Res. Eng. Technol.* **2013**, *2* (12), 625–635.

(2)   Andrew, R. M. Global CO2 Emissions from Cement Production. *Earth Syst.* **2018**, *10*, 195–217.

(3)   Alberto, A. S. C.; Rasteiro, M. G. Nanotechnology Applied to Chemical Soil Stabilization. *Adv. Transp. Geotech. 3* **2016**, *143*, 1252–1259.

(4)   Turkoz, M.; Savas, H.; Acaz, A.; Tosun, H. The Effect of Magnesium Chloride Solution on the Engineering Properties of Clay Soil with Expansive and Dispersive Characteristics. *Appl. Clay Sci.* **2014**, *101* (101), 1–9.

(5)   Rodriguez, A. K.; Ayyavu, C.; Iyengar, S. R.; Bazzi, H. S.; Masad, E.; Little, D.; Hanley, H. J. M. Polyampholyte Polymer as a Stabiliser for Subgrade Soil. *Int. J. Pavement Eng.* **2018**, *19* (6), 467–478.

(6)   Marto, A.; Latifi, N.; Eisazadeh, A. Effect of Non-Traditional Additives on Engineering and Microstructural Characteristics of Laterite Soil. *Arab. J. Sci. Eng.* **2014**, *39* (10), 6949–6958.

(7)   Blanck, G.; Cuisinier, O.; Masrouri, F. Soil Treatment with Organic Non-Traditional Additives for the Improvement of Earthworks. *Acta Geotech.* **2014**, *9* (6), 1111–1122.

(8)   Soon, N. W.; Lee, L. M.; Khun, T. C.; Ling, H. S. Improvements in Engineering Properties of Soils through Microbial-Induced Calcite Precipitation. *KSCE J. Civ. Eng.* **2013**, *17* (4), 718–728.

(9)   Kandasami, R. K.; Borges, R. M.; Murthy, T. G. Effect of Biocementation on the Strength and Stability of Termite Mounds. *Environ. Geotech.* **2016**, *3* (2), 99–113.

(10)   Jalili, M.; Ghasemi, M. R.; Pifloush, A. R. Stiffness and Strength of Granular Soils Improved by Biological Treatment Bacteria Microbial Cements. *Emerg. Sci. J.* **2018**, *2* (4), 219–227.

(11)   Lourenço, S. D. .; Wang, G. H.; Kamai, T. Water Repellent Soils for Slope Stability. In *XVI European Conference on Soil Mechanics and Geotechnical Engineering*; 2015.

(12)   Chang, I.; Im, J.; Cho, G. C. Introduction of Microbial Biopolymers in Soil Treatment for Future Environmentally-Friendly and Sustainable Geotechnical Engineering. *Sustainability* **2016**, *8* (3), 251.

(13)   I.Chang, J. Im, A. K. Pasidhi, G. C. C. Effects of Xanthan Gum Biopolymer on Soil Strengthening. *Constr. Build. Mater.* **2015**, *74*, 65–72.

(14)   Muguda, S.; Booth, S. J.; Hughes, P. N.; Augarde, C. E.; Perlot, C.; Bruno, A. W.; Gallipoli, D. Mechanical Properties of Biopolymer-Stabilised Soil-Based Construction Materials. *Géotechnique Lett.* **2017**, *7* (4), 309–314.

(15)   Tanaka, M.; Harlisa, I. H.; Takahashi, Y.; Ikhsan, N. A.; Okochi, M. Screening of Bacteria-Binding Peptides and One-Pot ZnO Surface Modification for Bacterial Cell Entrapment. *RSC Adv.* **2018**, *8* (16), 8795–8799.

(16)   Tanaka, M.; Alvin, A. W. L.; Okochi, M. Screening of Peptide Probe Binding to Particulate Matter with a High Metal Content. *RSC Adv.* **2018**, *8* (11), 5953–5959.

(17)   Tanaka, M.; Takahashi, Y.; Roach, L.; Critchley, K.; Evans, S. D.; Okochi, M. Rational Screening of Biomineralisation Peptides for Colour-Selected One-Pot Gold

Nanoparticle Syntheses. *Nanoscale Adv.* **2019**, *1* (1), 71–75.

(18) Tanaka, M.; Hikiba, S.; Yamashita, K.; Muto, M.; Okochi, M. Array-Based Functional Peptide Screening and Characterization of Gold Nanoparticle Synthesis. *Acta Biomater.* **2017**, *49*, 495–506.

(19) Tayebi-Khorami, M.; Edraki, M.; Corder, G.; Golev, A. Re-Thinking Mining Waste through an Integrative Approach Led by Circular Economy Aspirations. *Minerals* **2019**, *9* (5), 286.

(20) Rötzer, N.; Schmidt, M. Decreasing Metal Ore Grades—Is the Fear of Resource Depletion Justified? *Resources* **2018**, *7* (4), 88.

(21) Azam, S.; Li, Q. Tailings Dam Failures: A Review of the Last One Hundred Years. *Geotech. News* **2010**, *28*, 50-53

(22) Cambridge, M.; Shaw, D. Preliminary Reflections on the Failure of the Brumadinho Tailings Dam in January 2019. *Dams Reserv.* **2019**, *29* (3), 113–123.

(23) Kossoff, D.; Dubbin, W. E.; Alfredsson, M.; Edwards, S. J.; Macklin, M. G.; Hudson-Edwards, K. A. Mine Tailings Dams: Characteristics, Failure, Environmental Impacts, and Remediation. *Appl. Geochemistry* **2014**, *51*, 229–245.

(24) Chang, I.; Cho, G.-C. Shear Strength Behavior and Parameters of Microbial Gellan Gum-Treated Soils: From Sand to Clay. *Acta Geotech.* **2019**, *14* (2), 361–375.

(25) Chang, I.; Im, J.; Prasidhi, A. K.; Cho, G. C. Effects of Xanthan Gum Biopolymer on Soil Strengthening. *Constr. Build. Mater.* **2015**, *74*, 65–72.

(26) Gorakhiki, M. H.; Bareither, C. A. Sustainable Reuse of Mine Tailings and Waste Rock as Water-Balance Covers. *Minerals* **2017**, *7* (7), 128.

(27) Cornell, R. M. Influence of Organic Anions on the Crystallization of Ferrihydrite. *Clays Clay Miner.* **1979**, *27* (6), 402–410.

(28) International, A. *D2166/D2166M-16 Standard Test Method for Unconfined Compressive Strength of Cohesive Soil*; 2016.

(29) Colombo, C.; Palumbo, G.; Ceglie, A.; Angelico, R. Characterization of Synthetic Hematite (α-Fe2O3) Nanoparticles Using a Multi-Technique Approach. *J. Colloid Interface Sci.* **2012**, *374* (1), 118–126.

(30) Chernyshova, I. V.; Hochella Jr, M. F.; Madden, A. S. Size-Dependent Structural Transformations of Hematite Nanoparticles. 1. Phase Transition. *Phys. Chem. Chem. Phys.* **2007**, *9* (14), 1736.

(31) Ishikawa, T.; Takeuchi, K.; Kandori, K.; Nakayama, T. Transformation Of-FeOOH to-FeOOH in Acidic Solutions Containing Metal Ions. *Physicochem. Eng. Asp.* **2005**, *266*, 155–159.

(32) Maltas, E.; Ozmen, M. Spectrofluorometric and Thermal Gravimetric Study on Binding Interaction of Thiabendazole with Hemoglobin on Epoxy-Functionalized Magnetic Nanoparticles. *Mater. Sci. Eng. C* **2015**, *54*, 43–49.

(33) Mansfield, E.; Tyner, K. M.; Poling, C. M.; Blacklock, J. L. Determination of Nanoparticle Surface Coatings and Nanoparticle Purity Using Microscale Thermogravimetric Analysis. *Anal. Chem.* **2014**, *86* (3), 1478–1484.

(34) Riddick, T. *Control of Colloid Stability through Zeta Potential and Its Relationship to Cardiovascular Disease.*; Livingston Publishing: New York, 1968.

(35) Guan, X.; Chen, G.; Shang, C. ATR-FTIR and XPS Study on the Structure of

Complexes Formed upon the Adsorption of Simple Organic Acids on Aluminum Hydroxide. *J. Environ. Sci.* **2007**, *19* (4), 438–443.

(36) Shirajuddin, S.; Kamarun, D.; Thomas, S. Structural Elucidation of Galactomannan from 'Petai Belalang'(Leucaena Leucocephala) and Its Modified Analogue. *Int. J. Eng. Technol.* **2018**, *7* (4.18), 95–98.

(37) Qureshi, M. U.; Chang, I.; Al-Sadarani, K. Strength and Durability Characteristics of Biopolymer-Treated Desert Sand. *Geomech. Eng.* **2017**, *12* (5), 785–801.

(38) Johnson, S. B.; Brown, G. E.; Healy, T. W.; Scales, P. J. Adsorption of Organic Matter at Mineral/Water Interfaces. 6. Effect of Inner-Sphere versus Outer-Sphere Adsorption on Colloidal Stability. *Langmuir* **2005**, *21* (14), 6356–6365.

(39) Wei, W.; Petrone, L.; Tan, Y.; Cai, H.; Israelachvili, J. N.; Miserez, A.; Herbert Waite, J.; Wei, W.; Israelachvili, J. N.; Waite, J. H.; et al. An Underwater Surface-Drying Peptide Inspired by a Mussel Adhesive Protein. **2016**. https://doi.org/10.1002/adfm.201600210.

(40) Ma, X.; Pawlik, M. Role of Background Ions in Guar Gum Adsorption on Oxide Minerals and Kaolinite. *J. Colloid Interface Sci.* **2007**, *313*, 440–448. https://doi.org/10.1016/j.jcis.2007.04.075.

(41) Dogsa, I.; Tomšič, M.; Orehek, J.; Benigar, E.; Jamnik, A.; Stopar, D. Amorphous Supramolecular Structure of Carboxymethyl Cellulose in Aqueous Solution at Different PH Values as Determined by Rheology, Small Angle X-Ray and Light Scattering. *Carbohydr. Polym.* **2014**, *111*, 492–504.

(42) Oprea, A.-M.; Nistor, M.-T.; Profire, L.; Popa, M. I.; Lupusoru, C. E.; Vasile, C. Evaluation of the Controlled Release Ability of Theophylline from Xanthan/Chondroitin Sulfate Hydrogels. *J. Biomater. Nanobiotechnol.* **2013**, *04* (02), 123–131.

(43) Wong, J. W. C.; Ip, C. M.; Wong, M. H. Acid-Forming Capacity of Lead–Zinc Mine Tailings and Its Implications for Mine Rehabilitation. *Environ. Geochem. Health* **1998**, *20* (3), 149–155.

(44) Suleimanov, B. A.; Abbasov, H. F. Chemical Control of Quartz Suspensions Aggregative Stability. *J. Dispers. Sci. Technol.* **2017**, *38* (8), 1103–1109.

(45) Ferris, C. J.; Stevens, L. R.; Gilmore, K. J.; Mume, E.; Greguric, I.; Kirchmajer, D. M.; Wallace, G. G.; In Het Panhuis, M. Peptide Modification of Purified Gellan Gum. *J. Mater. Chem. B* **2015**, *3* (6), 1106–1115.

(46) Nickerson, M. T.; Paulson, A. T.; Hallett, F. R. Pre-Gel Solution Properties of Gellan Polysaccharides: Effect of Potassium and Calcium Ions on Chain Associations. *Food Res. Int.* **2008**, *41* (5), 462–471.

(47) Jain, V.; Tammishetti, V.; Joshi, K.; Kumar, D.; Pradip; Rai, B. Guar Gum as a Selective Flocculant for the Beneficiation of Alumina Rich Iron Ore Slimes: Density Functional Theory and Experimental Studies. *Miner. Eng.* **2017**, *109*, 144–152.

(48) Mercê, A. L. R.; Fernandes, E.; Mangrich, A. S.; Sierakowski, M. R.; Szpoganicz, B. Fe (III) - Galactomannan Solid and Aqueous Complexes: Potentiometric, EPR Spectroscopy and Thermal Data. *J. Braz. Chem. Soc.* **2001**, *12* (6), 791–798.

(49) Lal, R. *Principles of Soil Physics*; Marcel Dekker Inc: Ohio, 2004.

(50) Lalonde, K.; Mucci, A.; Ouellet, A.; Gélinas, Y. Preservation of Organic Matter in

Sediments Promoted by Iron. *Nature* **2012**, *483* (7388), 198–200.

(51) Barber, A.; Brandes, J.; Leri, A.; Lalonde, K.; Balind, K.; Wirick, S.; Wang, J.; Gélinas, Y. Preservation of Organic Matter in Marine Sediments by Inner-Sphere Interactions with Reactive Iron. *Sci. Rep.* **2017**, *7* (1).